PHYSICS AND CHEMISTRY OF SOLID STATE
V. 26, No. 4 (2025) pp. 844-851
Section: Technology

DOI: 10.15330/pcss.26.4.844-851

Vasyl Stefanyk Carpathian National University

ФІЗИКА І ХІМІЯ ТВЕРДОГО ТІЛА
Т. 26, № 4 (2025) С. 844-851
Технічні науки

PACS: 87.16.-b, 81.40.Ef, 62.20.mt

ISSN 1729-4428 (Print)
ISSN 2309-8589 (Online)

B.V. Efremenko[1], Yu.G. Chabak[2,1], E.V. Tsvetkova[1], I.M. Olejnik[1], V.G. Efremenko[2,1], A.V. Dzherenova[1]

Influence of annealing temperature on the Charpy fracture characteristics of selective laser melted 316L steel at ambient and cryogenic temperatures

[1]*Pryazovskyi State Technical University, Dnipro, Ukraine, vgefremenko@gmail.com*
[2]*Institute of Materials Research of Slovak Academy of Sciences, Kosice, Slovakia*

The effect of high-temperature annealing on the Charpy fracture properties of 316L stainless steel manufactured via Selective Laser Melting (SLM) was studied at ambient (25ºC) and cryogenic (–196ºC, LNT) temperatures. Charpy V-notched specimens (5×10×55 mm) were built along the Z-axis and annealed (5 h) at 900ºC, 1050ºC, or 1200ºC, followed by water quenching. Impact tests were performed with the force-displacement curves recording. Microstructure was analysed using OM, SEM, EBSD, and EDX. The SLM-316L exhibited impact toughness (KCV) of one-third that of rolled 316L due to SLM's cellular structure and specific micro-defects. Annealing at 900 ºC removed the cellular structure, slightly improving impact toughness, while annealing at 1200 ºC reduced it by a factor of 1.5 due to $(MnCrSiAl)O_3$ precipitation. At –196ºC, absorbed energy decreased compared to 25 ºC by a factor of 1.7-2.2. At 25ºC, crack propagation energy (KV_{prop}) exceeded crack initiation energy (KV_{ini}) across all conditions. At –196ºC, the KV_{prop} fraction in annealed samples decreased because of deformation-induced martensitic transformation. The cellular structure of as-printed steel promoted a higher KV_{prop} fraction at –196ºC. Ratio KCV_{LNT}/KCV_{RT} (0.46-0.59) indicates no ductile-brittle transition threshold, supporting the suitability of SLM-316L steel for cryogenic applications.

Keywords: 316L, Selective Laser Melting, annealing, impact toughness, absorbed energy, microstructure.

Received 13 August 2025; Accepted 25 November 2025.

Introduction

316L austenitic stainless steel (ASTM A240) is valued for its excellent mechanical properties, corrosion resistance, biocompatibility, and hypoallergenicity, making it a top choice for biomedical applications like orthopedic and cardiovascular implants, surgical and dental instruments, medical supplies, etc. [1]. 316L steel is produced using standard metallurgical technology (casting, rolling), with the final stage involving high-temperature processing (1050-1150ºC) followed by rapid cooling. This process, known as "solution annealing" [2], aims to achieve a homogeneous austenite structure and composition through dissolution of secondary phases (carbides, σ-phase, δ-ferrite) that degrade steel properties.

In recent decades, additive manufacturing technologies (AM) based on the use of powder materials [3, 4] have gained widespread development, enabling a substantial reduction in the production cycle for complex-shaped parts while minimizing material and energy costs. Among AM, 3D printing methods have gained the most popularity, particularly the selective laser melting method (SLM) [5-7]. Steel 316L is among the limited range of alloys used in the SLM process, making it of increased interest for research [8, 9]. Unlike rolled 316L, SLM-316L features a cellular microstructure that boosts strength but compromises ductility and impact toughness [10]. To achieve a more balanced set of mechanical properties, SLM-316L undergoes post-processing heat treatment similar to its rolled counterpart [9, 10]. While the effect of solution annealing on tensile properties of SLM-316L is well-documented [14-16], impact toughness (particularly

at cryogenic temperatures which is a key relevant domain for austenitic steels) remains much less studied [17-20]. For instance, Wang et al. [17] analyzed the impact toughness of SLM-316L steel based on the crystallographic orientation of printed samples, concluding that the <110> direction maximizes absorbed impact energy at both room temperature and liquid nitrogen temperature. Li et al. [18] stated that the deformation mechanism of 316L steel is temperature-dependent, with deformation-induced martensitic transformations occurring in the temperature range of 297 K to 15 K, reaching up to 13% at 15 K. Lou et al. [21] attributed the reduced impact toughness of SLM-316L steel after processing at 1066 °C to the formation of Si- and Mn-enriched oxide inclusions. In these studies, the impact toughness of SLM-printed steel was investigated either without post-processing heat treatment or with a single solution annealing regime. Furthermore, the influence of microstructure on the energy characteristics of the steel fracture process as a function of test temperature was not analyzed. Considering the above gaps, this study aims to determine the effect of the temperature of post-processing solution annealing on the impact toughness of SLM-manufactured 316L steel at ambient and cryogenic temperatures, with an emphasis on the relationship between microstructural changes and the ratio of absorbed impact energy expended on crack initiation and propagation.

I. Methods

Charpy specimens of 316L steel, sized 5×10×55 (mm), were fabricated using the selective laser melting technique, as detailed in [13]. During fabrication, the specimens' longitudinal axis was aligned with the build (Z) direction. The chemical composition of steel was 0.02 wt.% C, 16.39 wt.% Cr, 11.92 wt.% Ni, 2.36 wt.% Mo, 0.80 wt.% Si, 1.08 wt.% Mn, 0.007 wt.% S, and 0.018 wt.% P. The specimens were V-notched by a wire electrical discharge machine. As-built specimens (denoted AsB) were subjected to post-processing solution treatment at 900 °C, 1050 °C, and 1200 °C for 5 hours, quenched in water, and labeled A900, A1050, and A1200, respectively. Heat treatments were conducted in a muffle furnace with a 99.9 % pure nitrogen protective atmosphere. Post-treatment, specimens were ground with sandpaper to a surface roughness of R_a=0.2 μm to eliminate oxide layers and reduce manufacturing roughness. Charpy impact tests were carried out on a WANCE PIT602H-4 pendulum-type machine at 25 °C (room temperature, RT) and –196°C (liquid nitrogen temperature, LNT), with an absorbed energy (KV) and force-displacement curves recorded. For cryogenic tests, specimens were soaked in liquid nitrogen for 30 minutes prior to testing. Three samples were used for each regime, and the results were averaged. For microstructural examination, specimens were prepared by polishing with SiC papers and 1 μm diamond paste, followed by etching in a HCl/HNO_3 (3:1) mixture. Microstructures were observed using an Olympus GX71 optical microscope (OM) and a JEOL JSM-7000F field-emission scanning microscope (FE-SEM) with an Oxford Instruments INCAx-sight energy-dispersive X-ray (EDX) detector. Electron backscattering diffraction (EBSD) analysis was performed on a Thermo Fisher Scientific Apreo S Hivac FE-SEM with an Oxford Instruments EBSD Symmetry S3 system at 20 kV and a 0.5 μm step size. For transmission electron microscopy (TEM), a microscope JEOL JEM-F200 was used.

II. Results and Discussion

Fig. 1 shows Charpy impact test results for SLM-316L steel specimens. In the as-built state, specimens absorbed an average of 48.1 J at room temperature and 22.0 J at –196°C. After annealing at 900°C, the maximum absorbed energy values reached 51.0 J and 27.2 J, respectively, slightly exceeding those of the as-built specimens. At higher annealing temperatures, a progressive decrease in absorbed energy was observed, with the most significant (1.5-times) reduction at 1200°C (32.0 J at RT and 18.8 J at LNT). Overall, the KV variation profiles for different regimes were consistent for RT and LNT, though the difference between KV_{RT} and KV_{LNT} decreased as temperature rises. Accordingly, the KV_{LNT}/KV_{RT} ratio increased from 0.49 (AsB) to 0.59 (A1200). The reported KV values, adjusted for specimen cross-section, yield impact toughness values of 120 J/cm² for AsB and 128 J/cm² for A900, consistent with prior literature data for SLM-316L steel [19, 20], validating the conducted experiment. However, these values are approximately one-third of the impact toughness of rolled 316L steel which is 350-400 J/cm^2 [17, 22].

Fig. 1 illustrates impact curves plotted in "Force-Displacement" and "Force-Time" coordinates, revealing sequentially changing distinct stages (Fig. 1b): (a) an initial linear region of elastic deformation; (b) a sharp force dip due to inertial loading at elastic-to-plastic transition [23]; (c) a plastic deformation region starting at F_{gy} point; (d) a region of the crack propagation (starting from the maximum load (F_{max})). According to [24], the area under the curve for $F<F_{max}$ represents the crack initiation energy (KV_{ini}), while for $F>F_{max}$, it reflects the crack propagation energy (KV_{prop}). As seen in Fig. 1b, the experimental curves for the RT and LNT groups share a similar shape but differ significantly in numerical parameters: RT-tested specimens exhibit lower maximum force (7.3-7.6 kN) and greater displacement (impact duration), indicating more significant and prolonged deformation during fracture. In the RT group, the A1200 specimen, with the lowest F_{max} (7.3 kN), fractured in 1.6 ms at 8 mm displacement, 1.3-1.5 times faster than other specimens. The specimens AsB(RT), A900(RT) and A1050(RT) had comparable F_{max} (7.5-7.6 kN), with their curves closely resembling each other. The A900(RT) specimen exhibited the longest fracture duration (2.4 ms), achieving the greatest deformation of 12 mm. LNT group specimens displayed 1.2-1.4 times higher F_{max} (9.9-11.4 kN) and faster fracture, (4.0-5.5 ms), indicating easier crack propagation. Moreover, plastic deformation in LNT specimens began at higher F_{gy} (7.3-10.0 kN) compared to RT specimens (5.1-5.6 kN). Overall, the area under the curves closely correlated with the absorbed impact energy.

Fig. 2 presents data on the fractions of absorbed

energy spent separately on crack initiation (KV_{ini}) and crack propagation (KV_{prop}). RT group specimens exhibit higher crack propagation energy across all processing regimes, accounting for 54-59 % of the total absorbed energy (Fig. 2a). In the AsB(RT), A900(RT), and A1050(RT) specimens, the crack propagation energy remains at a consistent level, decreasing only in the A1200(RT) specimen. The ratio of crack initiation to propagation energy (KV_{ini}/KV_{prop}) varies within a narrow range, decreasing from 0.81-0.84 (AsB(RT), A900(RT)) to 0.69 (A1200(RT)) (Fig. 2b).

During cryogenic testing, only the AsB(LNT) specimen exhibits an KV_{ini}/KV_{prop} ratio consistent with the RT group trend. For annealed specimens, this ratio changes significantly: in A900(LNT) and A1050(LNT), KV_{ini} and KV_{prop} are nearly equal, while in the A1200(LNT) specimen, the crack initiation energy exceeds the crack propagation energy by 1.5 times (Fig. 2b).

All tested specimens showed similar fracture surface characteristics. At the macroscale, the fracture surface exhibited a coarse-crystalline appearance, consisting of terrace-like facets connected by steps and occasional dimple-like depressions (Fig. 3a). At the microscale, all specimens displayed a fine-dimpled structure with tear ridges along dimple edges, indicative of ductile mechanism of fracture (Figs. 3b-3h). In the AsB(RT) specimen, tear ridges aligned along cell boundaries, mirroring the cellular structure of the SLM specimen (Fig. 3b). Dimples initiated at non-metallic inclusions,

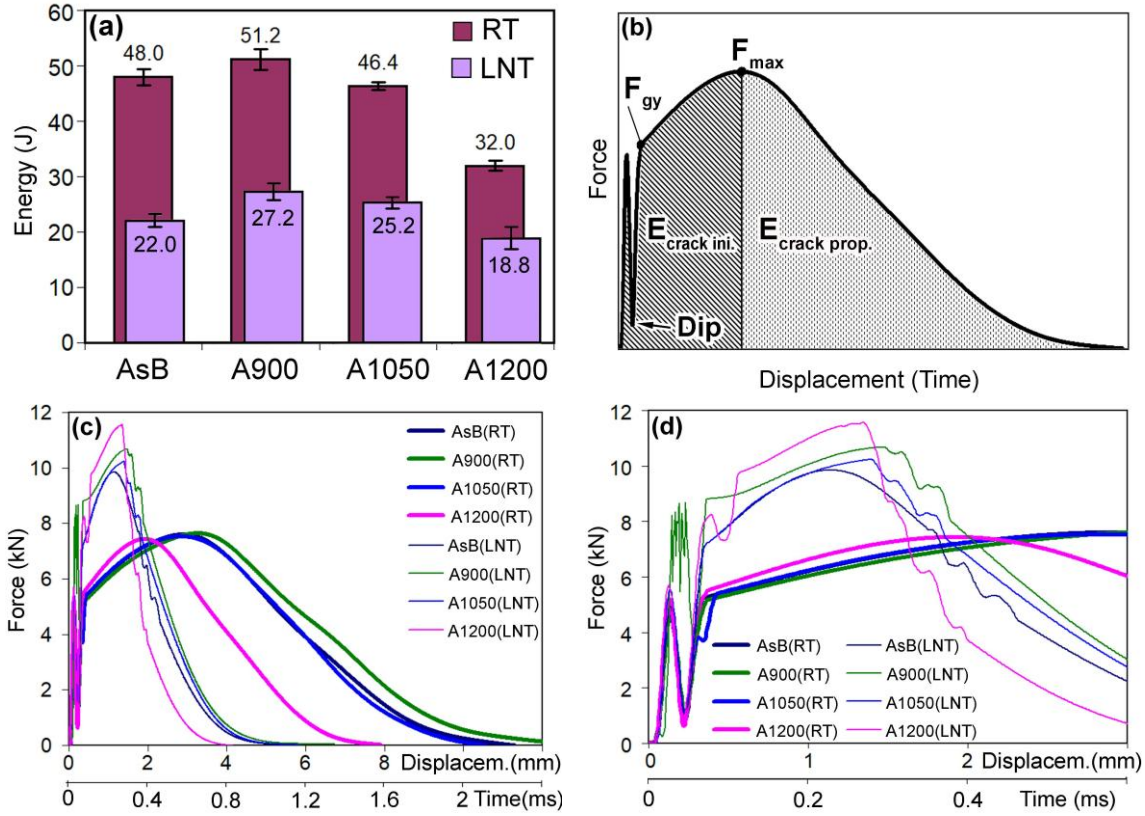

Fig. 1. (a) Total absorbed impact energy at room temperature and –196 ºC; (b) characteristic regions and points on the impact curve; (c) experimental impact curves of SLM-316L steel samples (general view); (d) detailed view of the curves at the initial stages of fracture.

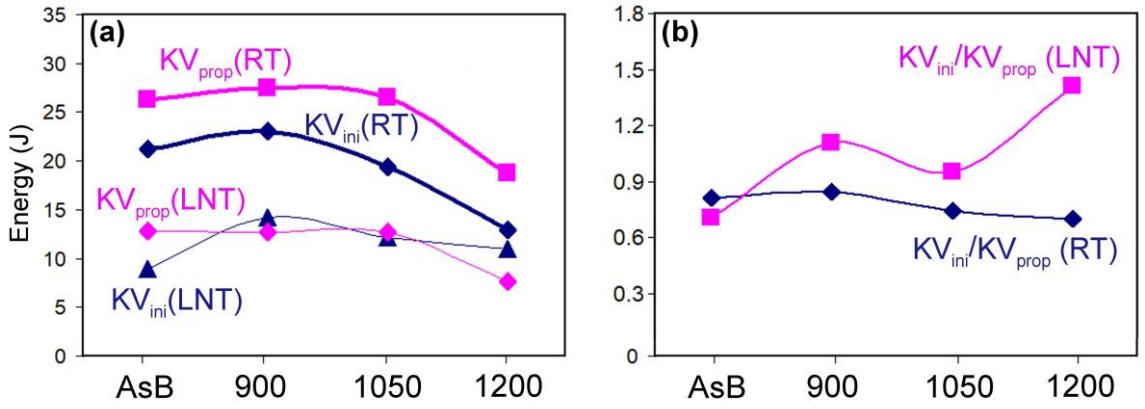

Fig. 2. Effect of annealing temperature on: (a) crack initiation energy (KV_{ini}) and crack propagation energy (KV_{prop}), (b) ratio KV_{ini}/KV_{prop}.

primarily complex manganese silicates $(MnCrSiAl)O_3$ [13], confirmed by point EDX analysis (the chemical composition of the inclusion shown in Fig. 3d is: 12.8 wt.% O, 4.4 wt.% Al, 7.5 wt.% Si, 13.3 wt.% Cr, 25.7 wt.% Mn, 36.3 wt.% Fe). A distinctive features of the A1200(RT) and A1200(LNT) specimens are the shallow dimples (indicating reduced energy absorption) and a high density of dimple initiation at oxide inclusions (shown the arrows in Fig. 3i).

The impact toughness behavior of the steel, as outlined above, resulted from structural transformation induced by heat treatment. Fig. 4a shows the initial (as-printed) microstructure of SLM 316L steel, characterized by rows of elongated elements with rounded contours, each representing a "melt pool" formed by the melting of powder under a laser beam during the printing process. The structure also contained typical SLM lack-of-fusion defects (pores) with a total area of 1.5-2.0%, as well as non-metallic inclusions ranging in size from 1.0 to 35.0 µm. The melt pools exhibited a fine columnar/cellular microstructure, typical of SLM alloys, composed of areas (bundles) of parallel cells extending tens of micrometers in length, with cross-sectional dimensions varying from 0.2 to 1.5 µm, depending on cell size and bundle orientation (Fig. 4b). Coarser cells (~2 µm) were observed at melt pool junctions. The cell walls, with thicknesses of 0.05-0.25 µm, were formed by dislocation clots and were enriched with Mo and Cr [4, 25]. Annealing at 900-1050 ºC led to the elimination of the cellular structure, although the melt pool regions retained their shape and crystallographic orientation (Figs. 4c and 4d). Increasing the annealing temperature to 1200 ºC initiated recrystallization, resulting in a microstructure more typical of FCC alloys: it consisted of remnants of melt pools and polyhedral recrystallized austenite grains, within which twins were observed (Fig. 4e). TEM studies revealed that in the samples annealed at 1200 ºC, unlike those at 900 ºC and 1050 ºC, a significant number of rounded non-metallic inclusions appeared, with sizes ranging widely from 0.02 to 0.5 µm (Fig. 4f) [13]. The similar processes of precipitation of dispersed particles (carbides, oxides, etc.) during high-temperature exposure are typically associated with a sharp decrease in corrosion resistance and impact toughness of alloys [26-28], particularly SLM-316L steel [13, 29, 30].

EBSD analysis of the fracture zone of the AsB(LNT) specimen revealed highly deformed "melt pool" regions, with no pronounced texture (Fig. 5a). Within the "melt pools", the slip band systems emerged, creating low-angle grain boundaries (LAGBs), the number of which exceeded high-angle grain boundaries (HAGBs) in a ratio LAGBs:HAGBs of 62:38 (Fig. 5b). This, in turn, led to significant local misorientation and the formation of strain localization zones at grain boundaries (shown in green in Fig. 5c). The calculated average Kernel Average Misorientation (KAM) value of 0.73 º indicates increased lattice distortion and a high density of geometrically necessary dislocations (GNDs) which appeared under

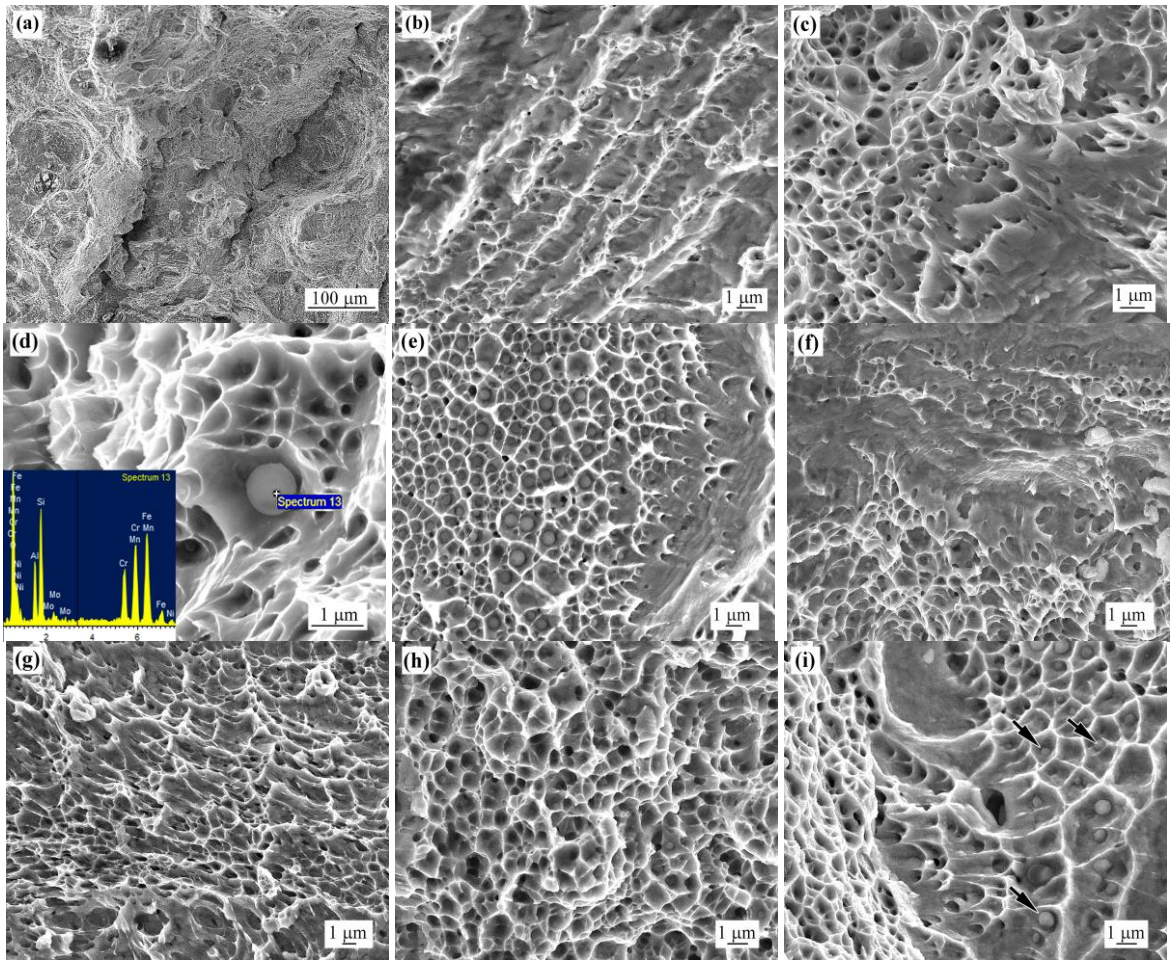

Fig. 3. Rupture surface of the specimens (a, b) AsB(RT), (c) A900(RT), (d) A1050(RT), (e) A1200(RT), (f) AsB(LNT), (g) 900(LNT), (h) A1050(LNT), (i) A1200(LNT).

fracture. This stressed state was further boosted by the deformation-induced martensitic γ→α′ transformation accompanying the rupture at low temperature, as evidenced by the appearance of BCC areas along slip lines (marked in red in Fig. 5d).

Conducted studies revealed that the impact toughness of SLM-316L steel in its as-printed state is significantly lower compared to rolled 316L, primarily due to SLM's specific cellular structure and defects, such as porosity and non-metallic inclusions. When tested at –196ºC, the absorbed energy decreased as expected, but the reduction was not drastic enough to indicate a distinct brittle-ductile transition threshold. High-temperature annealing failed to significantly enhance the toughness of SLM-316L steel: it slightly improved at 900 ºC but worsened at 1200ºC due to the formation of oxide inclusions.

The presence of defects arising from the SLM process (acting as the stress concentrators) made the crack

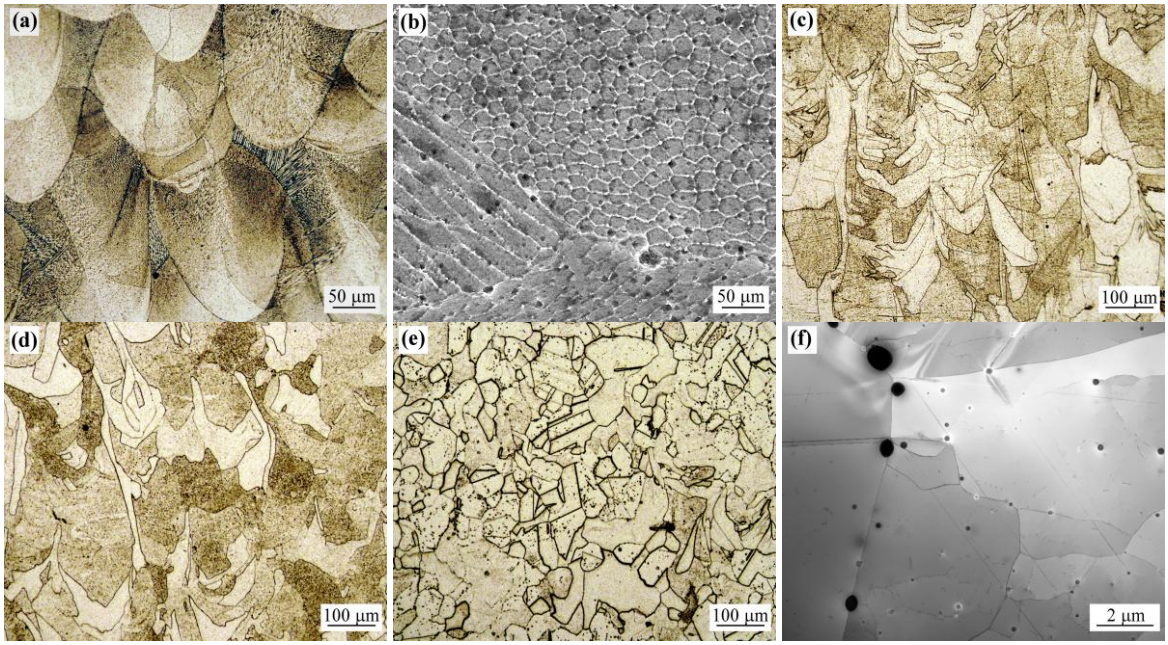

Рис. 4. Microstructure of the samples: (a, b) AsB(RT), (c) 900(RT), (d) 1050(RT), (e, f) 1200(RT). (a, c-e – OM, b – SEM, f – TEM).

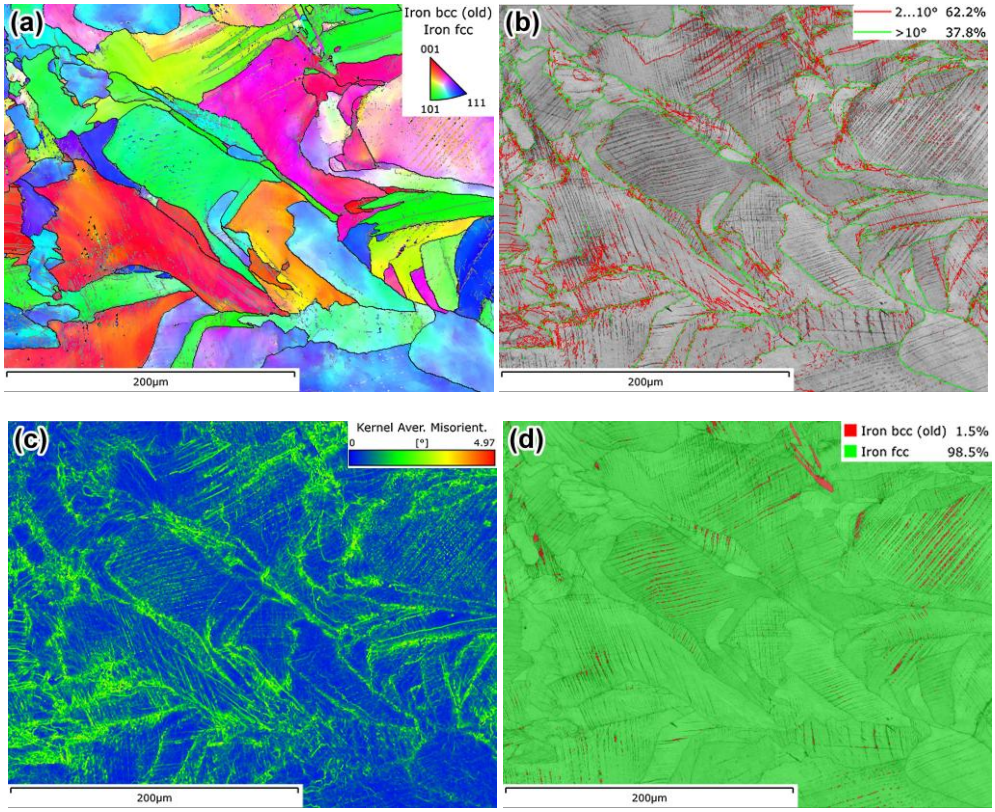

Рис. 5. The results of EBSD analysis of the AsB-LNT specimen: (a) Inverse Pole Figure map; (b) Grain Boundary map (green lines represent HAGBs, red lines represent LAGBs); (c) Kernel Average Misorientation map; (d) phase map (green represents FCC phase, red represents BCC phase).

initiations easier, therefore, at room temperature, the energy for crack propagation exceeded the energy for crack initiation. At –196°C, the proportion of KV_{prop} in annealed samples decreased, which can be explained by the work hardening and development of deformation-induced martensitic transformation, which generated the fields of elastic distortion ahead of the advancing crack front thus promoting its growth (Fig. 5c). In the AsB(LNT) sample, where KV_{ini}/KV_{prop} matched room temperature, the retention of a high proportion of KV_{prop} was presumably facilitated by the cellular structure, in which cell boundaries acted as barriers to the propagating crack [31].

Conclusions

The study on SLM-manufactured 316L stainless steel reveals that post-processing solution annealing diversely influences its Charpy impact toughness at both ambient (RT) and cryogenic (–196°C, LNT) temperatures. Annealing at 900-1050°C slightly enhances or maintains absorbed impact energy, with A900 specimens achieving the highest values (51.0 J at RT, 27.2 J at –196°C) which are one-third of rolled 316L. EBSD and TEM analyses confirm that higher annealing temperatures (1200°C) triggers recrystallization, altering the microstructure from cellular to polyhedral austenite grains; however, the impact toughness reduces (32.0 J at RT, 18.8 J at LNT) due to precipitation of manganese silicate $(MnCrSiAl)O_3$ inclusions, which act as stress concentrators. At 25°C, crack propagation energy (KV_{prop}) surpassed crack initiation energy (KV_{ini}) in all annealing regimes. At –196 °C, deformation-induced martensitic transformation in annealed samples lowers crack propagation energy, promoting crack growth. The as-built cellular microstructure enhances KV_{prop}, particularly at cryogenic temperatures, by acting as a barrier to crack growth. The ratio KCV_{RT}/KCV_{LNT} indicates no clear ductile-brittle transition threshold, confirming the suitability of SLM-316L steel for cryogenic applications.

Acknowledgements

This research was funded by the Ministry of Education and Science of Ukraine (project No. 0123U101834).

Efremenko B.V. – PhD, Associate Professor, Bio-Engineering Department;
Chabak Yu.G. – Dr. Sci, Professor, Physics Department;
Tsvetkova E.V. – PhD, Associate Professor, Physics Department;
Olejnik I.M. – PhD, Associate Professor, Head of Department of Materials Science
Efremenko V.G. – Dr. Sci, Professor, Head of Physics Department;
Dzherenova A.V. – Assistant Professor, Physics Department.

[1] N. M. Kibambe, B. A. Obadele, B. J. Babalola, U. S. Anamu, P. A. Olubambi, *Corrosion characteristics of heat-treated biomedical grade 316L stainless steel in simulated body fluids*. Results in Materials, 26, 100676 (2025); https://doi.org/10.1016/j.rinma.2025.100676.

[2] L. Gao, S. A. Mantri, X. Zhang, *Quantification of solution annealing effects on microstructure and property in a laser powder bed fusion 316H stainless steel*, Materials & Design, 251, 113692 (2025); https://doi.org/10.1016/j.matdes.2025.113692.

[3] G. Bagliuk, M. Marych, Y. Shishkina, A. Mamonova, O. Gripachevsky, S. Kyryliuk,. *Features of phase and structure formation in obtaining high-entropy alloy of Fe-Ti-Cr-Mn-Si-C system from a powder mixture of ferroalloys*. Physics and Chemistry of Solid State, 23(3), 620 (2022); https://doi.org/10.15330/pcss.23.3.620-625.

[4] V. Kulyk, I. Izonin, V. Vavrukh, R. Tkachenko, Z. Duriagina, B. Vasyliv, M. Kováčová, *Prediction of hardness, flexural strength, and fracture tiyghness of ZrO2 based ceramics using ensemble learning algorithms*, Acta Metallurgica Slovaca, 29 (2), 93 (2023); https://doi.org/10.36547/ams.29.2.1819.

[5] N. Haghdadi, M. Laleh, M. Moyle, S. Primig, *Additive manufacturing of steels: A review of achievements and challenges*, Journal of Materials Science, 56, 64 (2021); https://doi.org/10.1007/s10853-020-05109-0.

[6] V. G. Efremenko, A. G. Lekatou, Yu. G. Chabak, B. V. Efremenko, I. Petryshynets, V. I. Zurnadzhy, S. Emmanouilidou, M. Vojtko, *Micromechanical, corrosion and wet sliding wear behaviours of Co-28Cr-6Mo alloy: Wrought vs. SLM*, Materials Today Communications, 35, 105936 (2023); https://doi.org/10.1016/j.mtcomm.2023.105936.

[7] M. O. Vasylyev, B. M. Mordyuk, S. M. Voloshko, *Wire-feeding based additive manufacturing of the Ti–6Al–4V alloy. Part I. Microstructure*, Progress in Physics of Metals, 24 (1), 5 (2023); https://doi.org/10.15407/ufm.24.01.005.

[8] J. Yang, B. Li, Y. Zheng, G. Chen, X. Chen, *Low cycle fatigue behavior of additive manufactured 316LN stainless steel at 550 ◦C: Effect of solution heat treatment*. Int. J. Fatigue, 179, 108066 (2024); https://doi.org/10.1016/j.ijfatigue.2023.108066.

[9] B.V. Efremenko, V.I. Zurnadzhy, Yu. G. Chabak, V. G. Efremenko, K. V. Kudinova, V. A. Mazur, *A comparison study on the effect of counter ball material on sliding wear response of SLM-printed biomedical 316L steel*, Materials Today: Proceedings, 66, 2587 (2022); https://doi.org/10.1016/j.matpr.2022.07.112.

[10] O. O. Salman, C. Gammer, A. K. Chaubey, J. Eckert, S. Scudino, *Effect of heat treatment on microstructure and mechanical properties of 316L steel synthesized by selective laser melting*. Mater. Sci. Eng. A, 748, 205 (2019); https://doi.org/10.1016/j.msea.2019.01.110.

[11] E. Ura-Binczyk, A. Dobkowska, P. Bazarnik, J. Ciftci, A. Krawczynska, W. Chrominski, T. Wejrzanowski, R. Molak, R. Sitek, T. Płocinski, J. Jaroszewicz, J. Mizera, *Effect of annealing on the mechanical and corrosion properties of 316L stainless steel manufactured by laser powder bed fusion*. Mater. Sci. Eng. A, 860, 144263 (2022); https://doi.org/10.1016/j.msea.2022.144263.

[12] D. Kong, C. Dong, X. Ni, L. Zhang, J. Yao, C. Man, X. Cheng, K. Xiao, X. Li, *Mechanical properties and corrosion behaviour of selective laser melted 316L stainless steel after different heat treatment processes*. J. Mater. Sci. Technol., 35, 1499 (2019);

[13] B. Efremenko, Y. Chabak, I. Petryshynets, T. Zhao, V. Efremenko, K. Wu, T. Xia, M. Džupon, S. Arshad, *Evaluation of the Suitability of High-Temperature Post-Processing Annealing for Property Enhancement in SLM 316L Steel: A Comprehensive Mechanical and Corrosion Assessment*. Metals, 15, 684 (2025); https://doi.org/10.3390/met15060684.

[14] W. Liu, C. Liu, Y. Wang, H. Zhang, H. Ni, *Effect of heat treatment on the corrosion resistance of 316L stainless steel manufactured by laser powder bed fusion*. J. Mater. Res. Technol., 32, 3896 (2024); https://doi.org/10.1016/j.jmrt.2024.08.194.

[15] N. Abu-warda, J. Bedmar, S. García-Rodriguez, B. Torres, M.V. Utrilla, J. Rams, *Effect of post-processing heat treatments on the high-temperature oxidation of additively manufactured 316L stainless steel*. J. Mater. Res. Technol., 29, 3465 (2024); https://doi.org/10.1016/j.jmrt.2024.01.270.

[16] J. Bedmar, S. García-Rodríguez, M. Roldán, B. Torres J. Rams, *Effects of the heat treatment on the microstructure and corrosion behavior of 316L stainless steel manufactured by Laser Powder Bed Fusion*. Corros. Sci. 209, 110777 (2022); https://doi.org/10.1016/j.corsci.2022.110777.

[17] X. Wang, O. Sanchez-Mata, S.E. Atabay, J.A. Muñiz-Lerma, M.A. Shandiz, M. Brochu, *Crystallographic orientation dependence of Charpy impact behaviours in stainless steel 316L fabricated by laser powder bed fusion*, Additive Manufacturing, 46, 102104 (2021); https://doi.org/10.1016/j.addma.2021.102104.

[18] S. Li, P.J. Withers, S. Kabra, K. Yan, *The behaviour and deformation mechanisms for 316L stainless steel deformed at cryogenic temperatures*, Mater. Sci. Eng., A, Volume 880, 145279 (2023); https://doi.org/10.1016/j.msea.2023.145279.

[19] E. de Sonis, S. Dépinoy, P.-F. Giroux, H. Maskrot, P. Wident, F. Villaret, A.-F. Gourgues-Lorenzon, *Impact toughness at room and cryogenic temperatures of 316L stainless steel processed by wire arc additive manufacturing*, Mater. Sci. Eng., A, 933, 148276 (2025); https://doi.org/10.1016/j.msea.2025.148276.

[20] L. T. H. Nguyen, J. -S. Hwang, M. -S. Kim, J. -H. Kim, S. -K. Kim, J. -M. Lee, *Charpy Impact Properties of Hydrogen-Exposed 316L Stainless Steel at Ambient and Cryogenic Temperatures*. Metals, *9*, 625 (2019); https://doi.org/10.3390/met9060625.

[21] X. Lou, P.L. Andresen, R.B. Rebak, *Oxide inclusions in laser additive manufactured stainless steel and their effects on impact toughness and stress corrosion cracking behavior*, Journal of Nuclear Materials, 499, 182 (2018); https://doi.org/10.1016/j.jnucmat.2017.11.036.

[22] C.A. Sumanariu, C.G. Amza, F.Baciu, M.I. Vasile, A.I. Nicoara, *Comparative Analysis of Mechanical Properties: Conventional vs. Additive Manufacturing for Stainless Steel 316L*. Materials, 17, 4808 (2024); https://doi.org/10.3390/ma17194808.

[23] J. Mao, Q. Xu, J. Yang, C. Cao, D. Wang, F. Zhong, M. Chen, *Nonlinear Impact Damage Evolution of Charpy Type and Analysis of Its Key Influencing Factors*. Chinese Journal of Mechanical Engineering, 37, 3 (2024); https://doi.org/10.1186/s10033-023-00986-3.

[24] Y. Takashi, M. Nishioka, A. Kato, S. Hikasa, H. Iwabuki, K. Nagata, A. Asano, Atsushi. *Nano Structure of Polyketon/Polyamide Polymer Alloy,* Kobunshi Ronbunshu, 66(12), 577 (2009). https://doi.org/10.1295/koron.66.577.

[25] D. Riabov, A. Leicht, J. Ahlström, E. Hryha, *Investigation of the strengthening mechanism in 316L stainless steel produced with laser powder bed fusion*. Mater. Sci. Eng. A, 822, 141699 (2021); https://doi.org/10.1016/j.msea.2021.141699.

[26] O. V. Sukhova, V. A. Polonskyy, K. V. Ustinova, *Influence of Si and B on structure and corrosion properties of quasi-crystalline Al–Cu–Fe alloys in solutions of salts*, Metallofizika i Noveishie Tekhnologii, 40(11), 1475 (2018); https://doi.org/10.15407/mfint.40.11.1475.

[27] T. Loskutova, M. Scheffler, I. Pavlenko, K. Zidek, I. Pohrebova, N. Kharchenko, I. Smokovych, O. Dudka, V. Palyukh, I. Ivanov, Y. Kononenko, *Corrosion Resistance of Coatings Based on Chromium and Aluminum of Titanium Alloy Ti-6Al-4V*, Materials, 17(15), 3880 (2024); https://doi.org/10.3390/ma17153880.

[28] V.G. Efremenko, K. Shimizu, A. P. Cheiliakh, T. V. Kozarevs'ka, Yu. G. Chabak, H. Hara, K. Kusumoto, *Abrasive wear resistance of spheroidal vanadium carbide cast irons*. Journal of Friction and Wear, 34(6), 466 (2013); https://doi.org/10.3103/S1068366613060068.

[29] F. Yan, W. Xiong, E. Faierson, G.B. Olson, *Characterization of nano-scale oxides in austenitic stainless steel processed by powder bed fusion*, Scr. Mater., 155, 104 (2018); https://doi.org/10.1016/j.scriptamat.2018.06.011.

[30] E. de Sonis, S. Dépinoy, P.-F. Giroux, H. Maskrot, P. Wident, F. Villaret, A.-F. Gourgues-Lorenzon, *Microstructure – Toughness relationships in 316L stainless steel produced by laser powder bed fusion*, Mater. Sci. Eng., A, 877, 145179 (2023); https://doi.org/10.1016/j.msea.2023.145179.

[31] M. J. Paul, Q. Liu, X. Li, J. J. Kruzic, U. Ramamurty, B. Gludovatz, *Impact of micro and mesostructure on the fatigue crack growth in laser powder bed fusion fabricated AlSi10Mg*, Acta Materialia, 293, 121070 (2025); https://doi.org/10.1016/j.actamat.2025.121070.

Б.В. Єфременко[1], Ю.Г. Чабак[2,1], О.В. Цветкова[1], І.М. Олійник[1], В.Г. Єфременко[2,1], А.В. Джеренова[1]

Вплив температури відпалу на характеристики ударного руйнування сталі 316L, виготовленої методом селективного лазерного плавлення, за кімнатної та кріогенної температур

[1]*Приазовський державний технічний університет, Дніпро, Україна, vgefremenko@gmail.com*
[2]*Інститут матеріалознавства Словацької Академії наук, Кошице, Словаччина*

Досліджено вплив відпалу на характеристики руйнування нержавіючої сталі 316L, виготовленої селективним лазерним плавленням (SLM), при Шарпі випробуваннях за кімнатної та кріогенної (–196ºC) температур. Зразки розміром 5×10×55 мм були надруковані вздовж Z-напрямку та відпалені впродовж 5 год при 900ºC, 1050ºC та 1200ºC з гартуванням у воді. Ударні випробування за Шарпі (V-надріз) проводили з реєстрацією кривих «сила-переміщення». Мікроструктуру аналізували методами оптичної та електронної мікроскопії, мікродифракції (EBSD) та енергодисперсійного аналізу. Ударна в'язкість (KCV) SLM-316L сталі становила приблизно третину від катаного аналога через комірчасту структуру та дефекти, характерні для SLM процесу. Відпал при 900ºC усунув комірчасту будову, що незначно підвищило в'язкість; подальше зростання температури до 1200ºC знизило в'язкість в 1,5 рази через виділення силікатів $(MnCrSiAl)O_3$. При –196ºC загальна поглинена енергія удару знизилася відносно 25ºC у 1.7-2.2 рази. За температури 25ºC енергія розповсюдження ($KV_{розп}$) тріщини переважала енергію її зародження для усіх режимів обробки. При –196ºC частка $KV_{розп}$ у відпалених зразках зменшилась, що пов'язано з деформаційним мартенситним перетворенням $\gamma \rightarrow \alpha'$ при ударі. Комірчаста структура друкованої сталі сприяла збереженню високої частки $KV_{розп}$ за низької температури. Співвідношення KCV_{LNT}/KCV_{RT} (0,46-0,59) вказує на відсутність різкого порогу хладноламкості, що підтверджує придатність SLM-виготовленої 316L сталі для кріогенних застосувань.

Ключові слова: 316L, селективне лазерне плавлення, відпал, ударна в'язкість, поглинена енергія, мікроструктура.